Doping TiO$_2$ with Fe from iron rusty waste for enhancing its activity under visible light in the Congo red dye photodegradation

Endang Tri Wahyuni[*] , Novianti Dwi Lestari, Ibanez Rosesya Cinjana, Syafriyanti Annur, Taufik Abdillah Natsir and Mudasir Mudasir

*Correspondence:
endang_triw@ugm.ac.id

Department of Chemistry,
Faculty of Mathematics
and Natural Sciences, Universitas
Gadjah Mada, Yogyakarta,
Indonesia

Abstract

An afford to enhance TiO$_2$ activity under visible light as well as to utilize the iron rusty waste, has been conducted by doping Fe from the waste into TiO$_2$. The doping was performed by sol-gel method of titania tetra isopropoxide with Fe^{3+} ions dissolved from the iron rust waste. In the doping, the concentration of Fe^{3+} was varied giving various mole ratios of TiO$_2$:Fe. The doped TiO$_2$ photocatalysts were characterized using FTIR, XRD, SRUV, and SEM-EDX instruments. The photocatalytic activity of the doped TiO$_2$ was evaluated by photodegradation of Congo red under visible light. The effect of some parameters that govern the photodegradation process such as the amount of Fe dopant, reaction time, photocatalyst mass, solution pH, and initial concentration of dye was also studied. The characterization results reveal that Fe^{3+} ions from the rusty waste have been doped into TiO$_2$ which can remarkably narrow the band gap energy (Eg), shifting into the visible zone. In accordance, the activity of TiO$_2$ under visible light in the dye photodegradation is considerably enhanced. The Eg decreasing and actively improving the doped TiO$_2$ are controlled by the amount of Fe dopant, and the most effective Eg decreasing is shown by TiO$_2$–Fe (1:0.8), but the highest activity is observed for TiO$_2$–Fe (1:0.4). It is also found that the highest photodegradation of Congo red 5 mg/L in 50 mL of the solution over TiO$_2$–Fe (1:0.4) under visible light, that is about 99%, can be reached by applying 60 mg of the photocatalyst mass, in 60 min, and solution pH 5. It is implied that the rusty waste can be utilized to prepare the visible responsive photocatalyst that can be used for preventing dye pollution.

Keywords: TiO$_2$, Doping, Fe, Rusted iron waste, Congo red, Photodegradation

Introduction

TiO$_2$ nanoparticles have attracted considerable attention as a photocatalyst for the degradation of various organic pollutants [1–4]. Due to being stable, inexpensive, having high photocatalytic activity, nontoxicity, and electron transfer to molecular oxygen, TiO$_2$ has turned into one of the most popular photocatalysts [1–15]. Unfortunately, TiO$_2$ is a semiconductor with a large band gap energy (Eg) that is 3.2 eV for the anatase phase, which is equal to a wavelength of 387 nm, allowing it to have high activity only under UV light or be less active under visible light [5, 7–15]. This
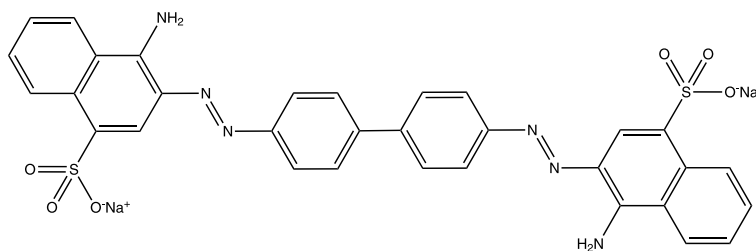
Wahyuni *et al. Journal of Engineering and Applied Science* (2023) 70:9

Page 2 of 14

Fig. 1 Chemical structure of Congo red

confines the application of TiO_2 under sunlight because sunlight only contains about 3–5% UV light and dominantly consists of visible light [5, 7]. Doping TiO_2 with transition metals is found as an intensive afford to extend and enhance TiO_2 activity under visible light [5, 7–15]. Among the transition metals, Fe dopant is reported to show a significant effect in improving TiO_2 activity [9–15]. The Fe^{3+} ion has a smaller ionic radius (0.64 Å) and electronic charge (3+) than that of Ti^{4+} (ionic radius = 0.68 Å with 4+ charge), enabling Fe^{3+} to easily substitute the Ti^{4+} ion from Ti–O–Ti [10, 11]. This substitution can create a new band occupying the conduction and valence bands, which remarkably narrows the gap [9–15].

In the Fe doping, the sources of Fe dopants frequently used are commercial pure salts such as $Fe(NO_3)_3$ [9–15], $FeSO_4$ [13], and $K_3Fe(CN)_6$ [12], that have a high price, leading to the doping process costly. Hence, finding a low-cost Fe source is beneficial, which can be obtained from iron rusty waste found easily in the environment. Rusted iron is an iron that undergoes oxidation by oxygen air and water, to form Fe_2O_3 [16–18]. This rust formation causes the iron material brittle [16], so it losses its function, and finally the material becomes useless solid waste. The presence of iron rusty waste in the environment can reduce aesthetics and potentially cause tetanus of the open hurt [18]. In fact, the iron rust waste with high Fe content can be utilized as a source of Fe dopant into TiO_2 resulting in the visible responsive photocatalyst. So far, doping TiO_2 with Fe from iron rusty waste is untraceable.

In this present work, the use of iron rust waste as a source of Fe dopant for enhancing the TiO_2 activity under visible light is systematically addressed. The effect of Fe doping on the photocatalyst performance under visible light was evaluated through Congo red dye photodegradation by laboratory experimental. The Congo red dye ($C_{32}H_{22}N_6Na_2O_6S_2$), as seen in Fig. 1, is sorted as a pollutant model due to its widely used in the textile and other wearable industries [19–22], and biochemical laboratories [23]. The intensive use of the dye must release a large volume of wastewater containing high dye levels. The Congo red dye contamination adheres to the ecosystem and human health, since it is able to destroy biotics as well as causes nausea, vomiting, and diarrhea [19–22], event induces cancer for humans. Various methods have been reported for diminishing the dye such as adsorption [19], biodegradation [20], ozonation [21], photo-Fenton [22, 23], and photocatalytic degradation over Fe-doped TiO_2 [24]. However, photodegradation over TiO_2 doped with Fe from the iron rusty waste has not been explored yet.

In the photodegradation of the Congo red dye over the Fe-doped TiO_2 photocatalyst, various variables such as the amount of Fe doping concentration, pH of the dye

Wahyuni *et al. Journal of Engineering and Applied Science*   (2023) 70:9

Page 3 of 14

solution, photocatalyst mass, contact time, and initial concentration of the Congo red dye are optimized to obtain the best condition of the dye removal.

Experimental

Material

The materials used in this study were Titanium (IV) isopropoxide (TTIP) 97%, ethanol (C_2H_5OH) 95%, hydrogen chloride (HCl) 35%, nitric acid (HNO_3) 68%, sodium hydroxide (NaOH) with the pro analysis (p.a) grade that was used as received. In addition, iron rusty solid waste taken from around Yogyakarta City was also employed.

Instruments

Visible light (Philips 36 W) and UV light lamps (Philips 160 W) were used as the light source for the photocatalysis process. The instruments operated for analysis and characterization included UV-visible spectrophotometer (Analytic Jena), specular reflectance UV-visible spectrophotometer (SR UV-Vis, Shimadzu UV-1700 Pharma Spec), Fourier-transform infrared spectrophotometer (FT-IR) (Shimadzu Prestige-21), X-ray diffraction (XRD, Rigaku Multibox 2 kW), and scanning electron microscope with energy dispersive X-ray spectrophotometer (SEM-EDX, Phenom-World).

Methods

Preparation of the Fe-doped TiO_2

Doping TiO_2 with Fe atoms was conducted by using sol-gel method, that was by interacting the TTIP solution with the solution containing Fe^{3+} dissolved from the iron rusty waste. The Fe^{3+} solution was prepared by dissolving 0.80 grams of the iron rusty waste in 7.5 ml of aqua regia (a mixture of concentrated HCl and HNO_3 with volume ratio of 3:1) to form a brown clear solution indicating the presence of Fe^{3+} ions, then the solution was diluted into 100 mL. The concentration of Fe^{3+} in the solution determined by using AAS was found as much as 0.05 mmole/mL.

At the same time, 10 ml of TTIP 1 mole/L was dissolved in 30 mL of ethanol while being stirred magnetically for 15 min to get a clear solution. Five beaker glasses containing 10 mmole of the TTIP were added with 1, 2, 4, 10, and 20 mL respectively, and were continued by the addition of acetic acid to get pH 3 along with magnetic stirring for 3 h to get a clear homogenous solution. Then the clear solutions were cooled in the refrigerator for 24 h so that the gel phase was produced. The gels were calcined at 500 °C for 3 h, and so the powder samples were obtained as the Fe-doped TiO_2 photocatalysts. The doped photocatalysts obtained were notified as TiO_2–Fe (1:0.05), TiO_2–Fe (1:0.1), TiO_2–Fe (1:0.2), TiO_2–Fe (1:0.5), and TiO_2-Fe (1:1) following the mole ratio of Ti to Fe.

Characterization

The doped-TiO_2 photocatalyst powders were characterized by using several instruments including SR-UV/Visible, FTIR, XRD spectrometers, and SEM-EDX. The SR-UV/Visible spectra of the samples were taken from 200 to 800 nm of the wavelength. The FTIR spectra were scanned in the range of 4000–400 cm^{-1} of the wavenumbers. The XRD patterns were recorded on the instrument using Cu-Kα as an X-ray source, from 3 to 50°

Wahyuni *et al. Journal of Engineering and Applied Science*   (2023) 70:9

Page 4 of 14

of the two tetha. The SEM images along with the EDX spectra were shot from the microscope with × 10,000 magnification.

Photoactivity assessment

In this typical, a series of 6 dye solutions as much as 50 mL having 10 mg/L of the dye concentration at pH 5, were added with 40 mg of the un-doped, and the doped TiO_2 photocatalysts with various Fe amounts. The mixtures were placed in a closed box equipped with visible lamps and then were irradiated with the visible light accompanied by stirring magnetically for 60 min. After the desired time, the mixtures were filtered to get the clear filtrates of the LAS solutions. The clear solutions were analyzed by using a UV-visible spectrophotometer based on the reaction with methylene blue and extraction with chloroform solvent. The blue solution absorbance was then measured at 499 nm. The absorbance observed then was interpolated into a respective standard curve to get the dye concentration left in the solution. The amount of dye degradation presented in % was determined by the following relationship:

$$E = \frac{C_0 - C_f}{C_0} \times 100\%$$

$E =$ the amount of dye degraded (%)$C_o =$ initial amount of the dye (mg)$C_f =$ the amount of dye undegraded or left in the solution after photodegradation (mg)

The same procedure was repeated with different conditions, including irradiation time (5, 15, 30, 45, 60, 75, 90, and 120 min), photocatalyst weight (10, 20, 30, 40, 60, 80, and 100 mg), solution pH (1, 3, 4, 5, 7, and 9), as well as the dye initial concentration (5, 10, 25, and 50 mg/L), where the volume of the dye solution was set to be 50 mL. When one variable was varied, the other variables were kept to be constant.

Result and discussion

Characterization results

SR-UV/visible data

The SR-UV/visible spectra of the photocatalysts are illustrated in Fig. 2. It is seen in the figure, that the Fe-doped TiO_2 samples show their absorption edge at the longer wavelengths (λ), entering the visible region than the absorption of the undoped one. This absorption shifts allowing the doped TiO_2 to strongly absorb the visible light, which is hoped to show higher activity in the presence of visible light.

The wavelengths of the absorption edge of all samples were presented in Table 1, along with the band gap energy (Eg) values that were calculated by the Tauc plot method as seen in Fig. 3. The data in Table 1 illustrates that Fe doping results in a decrease in the band gap energy (Eg) of TiO_2 from 3.15 eV to 3.05–2.38 eV. With the higher amount of Fe dopant, the lower Eg values are observed. Similar data have also been reported previously [5–15]. The Eg reduction is caused by the narrowing gap in the TiO_2 semiconductor structure due to the new band formation located between the valence and conduction bands. The new band generated by the dopant clearly notifies that the Fe^{3+} in the solution has been successfully doped [14]. Generally, the remarkable Eg decrease can also imply that the Fe doping into the TiO_2 structure follows the interstitial mechanism [15].
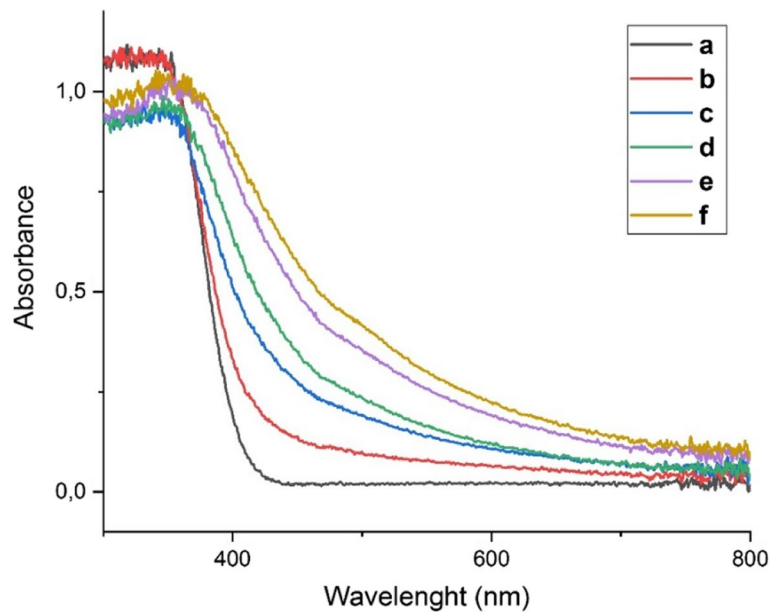
Fig. 2 The SR-UV/Visible spectra of **a** TiO_2, **b** TiO_2–Fe(1:0.05), **c** TiO_2–Fe(1:0.1), **d** TiO_2–Fe (1:0.2), **e** TiO_2–Fe(1:0.5), and **f** TiO_2–Fe (1:1)
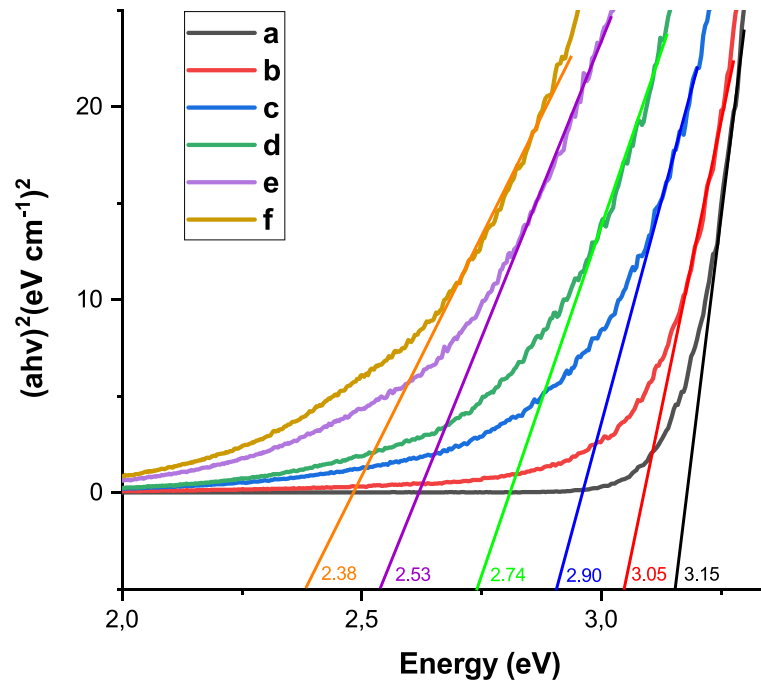
Fig. 3 The Tauc Plot of **a** TiO_2, **b** TiO_2–Fe(1:0.05), **c** TiO_2–Fe(1:0.1), **d** TiO_2–Fe (1:0.2), **e** TiO_2–Fe(1:0.5), and **f** TiO_2-Fe (1:1)

FTIR data

In Fig. 4, the FTIR spectra of the Fe-doped TiO_2 photocatalysts are seen similar to the spectra of the undoped one. The appearance of the peaks at the wavenumbers of 3749–3425 cm^{-1} and 1635 cm^{-1}, assign respectively the stretching and bending

Table 1 Band gap (Eg) energy values of the TiO_2 and TiO_2–Fe

Photocatalyst	λ (nm)	Band gap (Eg)
TiO_2	412	3.15
TiO_2–Fe(1:0.05)	424	3.05
TiO_2–Fe(1:0.1)	459	2.90
TiO_2–Fe(1:0.2)	490	2.74
TiO_2–Fe(1:0.5)	536	2.53
TiO_2–Fe(1:1)	554	2.38
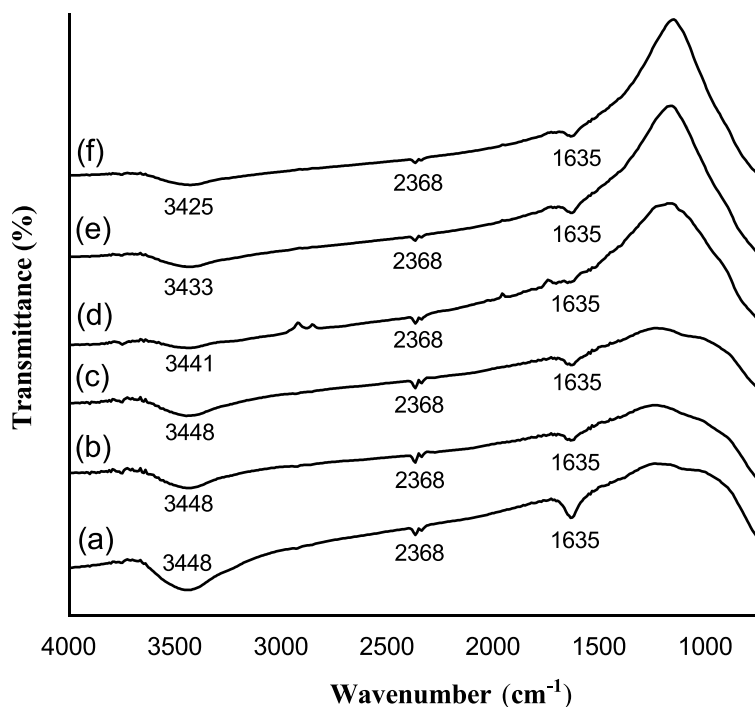
Fig. 4 FTIR spectra of **a** TiO_2, **b** TiO_2–Fe(1:0.05), **c** TiO_2–Fe(1:0.1), **d** TiO_2–Fe(1:0.2), **e** TiO_2–Fe(1:0.5), and **f** TiO_2–Fe(1 :1)

vibrations of O–H from H_2O adsorbed on the surface of the photocatalyst [14]. The characteristic peak of TiO_2 appears in the wavenumber of 400–800 cm^{-1}, representing the Ti–O–Ti or O–Ti–O vibrations [5, 14].

In the spectra of all TiO_2–Fe samples, peaks at around 450–493 cm^{-1} can be seen, which are the shifts from the peak of 509 cm^{-1} belonging to the undoped TiO_2. The shifts can indicate the disturbance of the Ti–O–Ti bond by the Fe dopant, due to the interaction between oxygen atoms in the Ti–O–Ti bond with the Fe doped [14]. Such interaction indicates the occurrence of the interstitial doping mechanism [14, 15].

XRD data

The XRD patterns of the undoped TiO_2 and all of the TiO_2–Fe photocatalysts were displayed in Fig. 5. The characteristic peaks of TiO_2 appear at the 2θ angles of 25.18°; 38.26°;

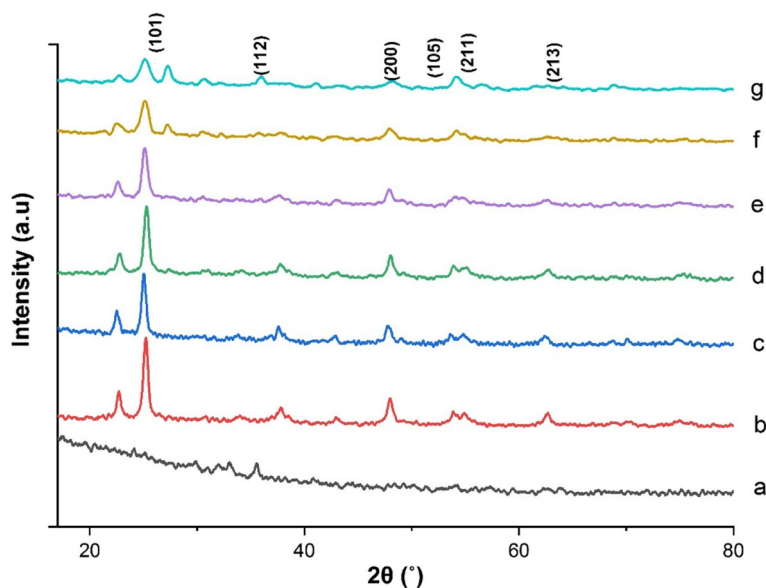**Fig. 5** X-ray diffraction patterns of **a** Fe_2O_3, **b** TiO_2, **c** TiO_2–Fe(1:0.05), **d** TiO_2–Fe(1:0.1), **e** TiO_2–Fe(1:0.2), **f** TiO_2–Fe(1:0.5), and **g** TiO_2–Fe(1:1)

Table 2 Effect of Fe doping on the average crystallite size of TiO_2

TiO_2 photocatalyst	The average crystallite size (nm)
TiO_2	66.65
TiO_2–Fe(1:0.05)	61.72
TiO_2–Fe(1:0.1)	60.15
TiO_2–Fe(1:0.2)	57.98
TiO_2–Fe(1:0.5)	55.84
TiO_2–Fe(1 :1)	26.16

47.7°; 54.44°; 55.26°; 62.52°, which good match with TiO_2 anatase crystal data as listed in COD CIF File No.: 00-152-6931 with the Miller index (hkl) to (101), (112), (200), (105), (211), and (213) respectively [5, 12].

Further, it is clearly observed that all TiO_2-Fe samples with various Fe content have similar patterns as the undoped TiO_2 pattern, but with lower intensities and without any new pattern of the dopant. This finding suggests that Fe doping gives no effect on the crystal phase change, as also reported previously [9, 13–15]. The lower intensities refer that the doped TiO_2 is in the less crystalline phase, due to the inhibition of the TiO_2 crystallinity growth [15]. Such inhibition of the crystallographic growth is most probably affected by the Fe dopant inserted in the TiO_2 crystal lattice, which was well documented in previous works [15]. Then, the absence of the dopant pattern implies that the Fe dopant has been successfully incorporated into the crystal lattice of TiO_2 due to the nearly identical ionic radius to that of the Ti^{4+} cation (0.0745 nm) [15]. In addition, the data in Table 2 demonstrates that the Fe doping has dismissed the average crystal sizes of TiO_2, and the gradual size reduction is observed as the amount of the dopant is increased. The decreasing crystal

size due to the Fe doping may indicate that the doping takes place through the substitution of the Ti atom in Ti–O–Ti by Fe dopant possessing smaller ionic radii (0.64 A) than that of Ti (0.68) [15]. This reason is clearly supported by the fact that more amount of Fe dopant in TiO_2–Fe strongly depresses the crystallite size.

TEM images

The TEM image of undoped TiO_2 shows cleaner spheres, while Fe-doped TiO_2 appears as darker-colored spheres, as illustrated by Fig. 6. The dark color in the TEM image illustrates the presence of Fe dopant atoms that have successfully entered the crystal lattice of TiO_2. Other Authors have also reported similar images [14].

The activity of the Fe- doped TiO_2
Effect of the dopant amount

The effect of Fe doping on the CR dye photodegradation is illustrated in Fig. 7. It is seen in the figure that Fe doping has considerably enhanced the TiO_2 activity in dye degradation, both under UV and visible light. Moreover, as the Fe dopant amount is enlarged, the higher activity is notified, but the opposite data is observed for the further increase of the Fe amount.

The enhancement of the dye photodegradation under visible light, over the undoped TiO_2, is induced by the larger ability of the doped TiO_2 in the visible absorption due to their lower Eg corresponding to visible photon energy. With such Eg values, TiO_2 can be activated by visible light to form holes and electrons. The holes then are scavenged by H_2O molecules that become OH radicals, while the electrons can be captured by dissolved oxygen to form superoxide ($\cdot O_2$) radicals. These radicals act as strong oxidizing agents that are responsible for dye degradation [5]. The reactions of radical formation and dye degradation are presented below:
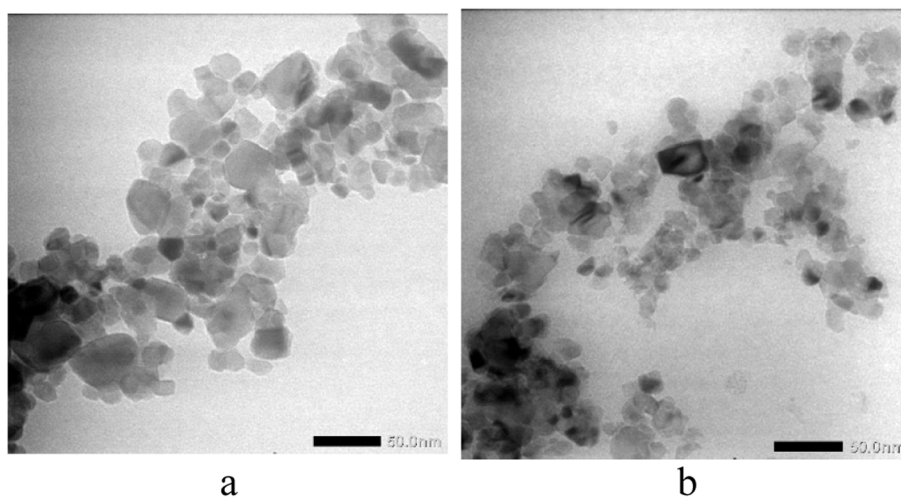
$$TiO_2 + h\nu \rightarrow TiO_2 \left(e^- + h^+ \right) \tag{1}$$

Fig. 6 The TEM images of **a** TiO_2 and **b** TiO_2 –Fe 1:0.5
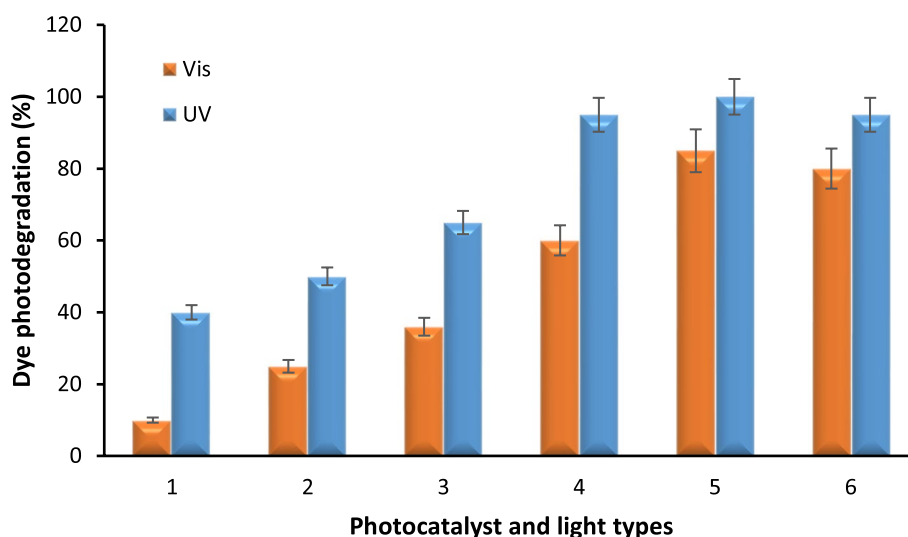
Fig. 7 The dye photodegradation over: **1** TiO_2, **2** TiO_2–Fe(1:0.05), **3** TiO_2–Fe(1:0.1), **4** TiO_2–Fe(1:0.2), **5** TiO_2–Fe(1:0.5), and **6** TiO_2–Fe(1:1) under visible and UV lights. (Dye concentration $= 10$ mg/L, dye solution volume $= 50$ mL photocatalyst weight $= 40$ mg, irradiation time $= 60$ min, and pH $= 5$)

$$h^+ + H_2O \rightarrow H^+ + \bullet OH \tag{2}$$

$$e^- + O_2 \rightarrow \bullet O_2 \tag{3}$$

$$C_{32}H_{22}N_6Na_2O_6S_2 + \bullet OH \rightarrow CO_2 + H_2O + Na_2SO_4 + HNO_3 \tag{4}$$
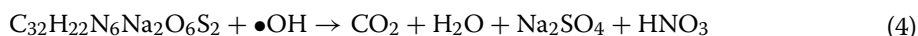
As the Fe amount increases, the larger visible light can be absorbed, which produces more radicals, which is a very conducive condition for dye photodegradation. The enhancement of the degradation is advanced to proceed up to reach the maximum level. However, the amount of Fe exceeding the optimum level leads to the degradation being dismissed. A large amount of Fe dopant may form the aggregate with a larger size covering the active surface of TiO_2, which prevents the direct contact of light with the photocatalyst. As a consequence, the less OH radicals can be produced.

The activity of the doped-TiO_2 under UV light is also found to be higher than that of the undoped photocatalyst. The presence of the Fe dopant in the structure of the TiO_2 crystal creating a new band can capture the electrons excited from the valence band [15]. Consequently, the recombination of holes and electrons can be delayed, so that more holes and radicals are available. This situation can promote more effective dye degradation. Further enhancement of the degradation is notified as the number of dopants increases, which should be resulted from the greater prevention of the recombination. Unfortunately, the TiO_2–Fe(1:1) with the highest fraction of the Fe dopant, possessing a very narrow gap, as indicated by the lowest Eg, can facilitate the electrons and holes to recombine. In other words, a very large dopant amount in TiO_2 can act as a recombination center. Hence, in the degradation process is a lack of holes and OH radicals, giving low degradation.

Effect of the irradiation time

It is demonstrated in Fig. 8, that the improvement of the dye photodegradation can be resulted as the irradiation is extended from 5 to 60 min, but the longer time than 60 min gives no effect on the degradation. Prolonged irradiation time enables more effective contact between the visible light with the photocatalyst, resulting in a larger number of holes and OH radicals. In addition, with a longer time, the contact between the OH radicals with the dye can intensively occur. These situations are conducive to the dye degradation process. After 60 min running, the photocatalyst may be saturated that is not able to release more OH radicals, providing the same radicals quantity. This explains why the photodegradation remains the same although the irradiation time is extended up to 120 min.

Effect of the photocatalyst mass

Figure 9 displays the dye photodegradation resulted from the process using various masses of the photocatalysts under visible exposure. It is notified that the dye degradation sharply increases with the increase of photocatalyst masses, due to the larger number of OH radicals provided by more quantity of the photocatalyst. The contradiction trend is observed when the photocatalyst mass was further enlarged. The excessive amount of the photocatalyst creates higher turbidity in the dye solution, which hinders visible light penetration. Such less penetrated light may prevent the TiO_2 to devote more OH radicals, and so the lesser effective degradation is obtained.

Effect of the solution pH

The trend of the dye photodegradation results at the pH alteration was displayed in Fig. 10. The solution pH determines the charges of both TiO_2 and Congo red dye. The pH of the zero point charge of TiO_2 is reported as 6.5, where TiO_2 is in the neutral charge. It is assigned that at lower pH than 6.5, TiO_2 has a positive charge, while at pH higher than 6.5, the positive charge is formed on the TiO_2 surface [1, 2]. Congo red dye
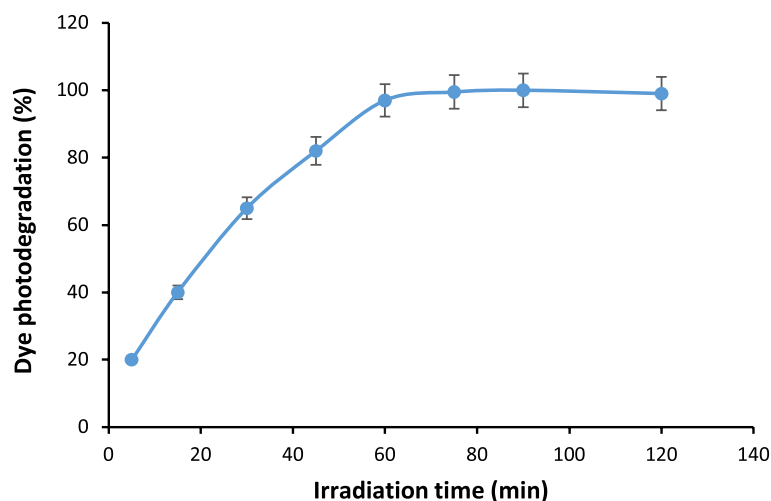

Fig. 8 Effect of the irradiation time on the dye photodegradation over TiO_2–Fe (1:0.5) under visible light. (Dye concentration = 10 mg/L, dye solution volume = 50 mL photocatalyst weight = 40 mg, and pH = 5)
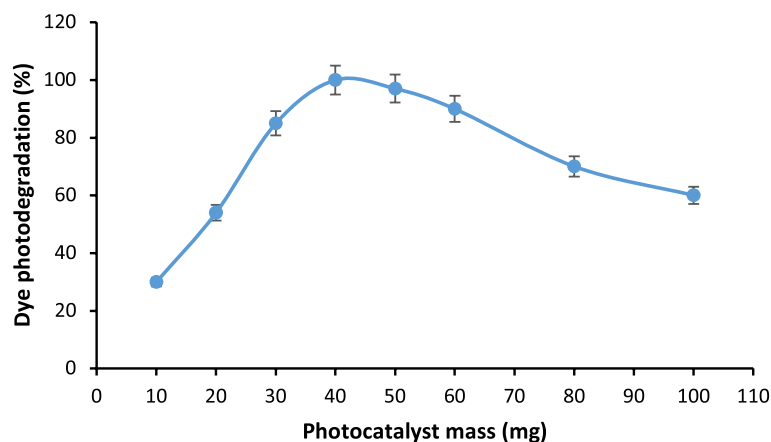
Fig. 9 Effect of the photocatalyst mass on the dye photodegradation over TiO_2–Fe (1:0.5) under visible light. (Dye concentration = 10 mg/L, dye solution volume = 50 mL irradiation time = 60 min, and pH = 5)
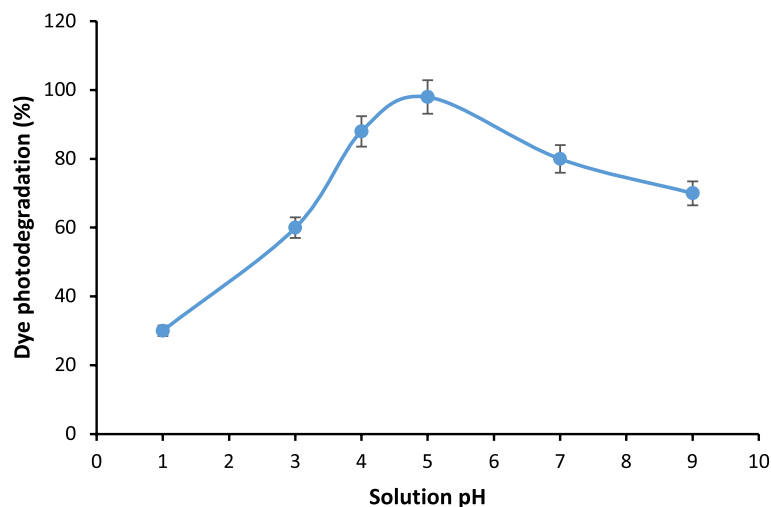

Fig. 10 Effect of solution pH (dye concentration = 10 mg/L, dye solution volume = 50 mL photocatalyst weight = 40 mg, and irradiation time = 60 min)

has an isoelectric charge at pH 3, suggesting that at pH lower than 3, the dye has a positive charge, and it will have a negative charge at pH higher than 3 [19].

From Fig. 9, it can be seen that at very low pH, the dye degradation is less effective. In this condition (pH 1), both TiO_2 and the dye have positive charges resulting from the protonation by a large number of H^+ ions. Consequently, there is a repulsion effect for the interaction between TiO_2 and the dye, giving low adsorption of the dye on the TiO_2 surface. Besides, in the protonated form, TiO_2H^+ is confined to release electrons and holes, which further reduces the OH radicals production. These conditions are less conducive to dye degradation.

When the pH is increased to 3, the degradation also rises. In this pH, the dye has no charges or is in the neutral species, and the TiO_2 is kept to be protonated, allowing TiO_2 to adsorb the dye but must be in the small portion. By elevating the media pH from 3 to 5, the protonated TiO_2 particles are still present in the large number, while

the dye molecules are dominantly in the negative charge. Thus, the dye adsorption and so dye degradation takes place effectively, and even reach the maximum degradation. It is observed that at higher pH than 5, the dye degradation gradually decreases. In the media with pH 7–9, both TiO_2 and the dye are negatively charged, causing a repulsive effect in the dye adsorption on the TiO_2 surface. Accordingly, it is reasonable therefore that the low dye degradation is the result.

Effect of the initial dye concentration

As appeared in Fig. 11, the dye degradation gradually declines when the dye's initial concentration is gradually elevated. The complete dye degradation is only observed for 5 mg/L of the concentration, and with 10 mg/L, the dye degradation is insignificantly different from the 5 mg/L. The photocatalyst is found to be less effective in dye degradation with higher dye concentrations. In that situation, the OH radicals from the same photocatalyst masses, are constant, while the dye molecules are in higher amounts, leading to a decrease in the dye photodegradation [25].

Stability test of the TiO_2–Fe

The stability of the TiO_2–Fe has been checked by measuring the concentration of the Fe dissolved from the photocatalyst during the dye photocatalytic degradation process. The photocatalyst tested was TiO_2–Fe (1:0.5) showing the best performance, and the results are presented in Fig. 12. It is seen in the figure that during the photocatalysis degradation, a very low amount of Fe dissolved is detected. The longer the irradiation time, the Fe dissolved is slightly increased. It is believed hence that the Fe dopant has high stability.
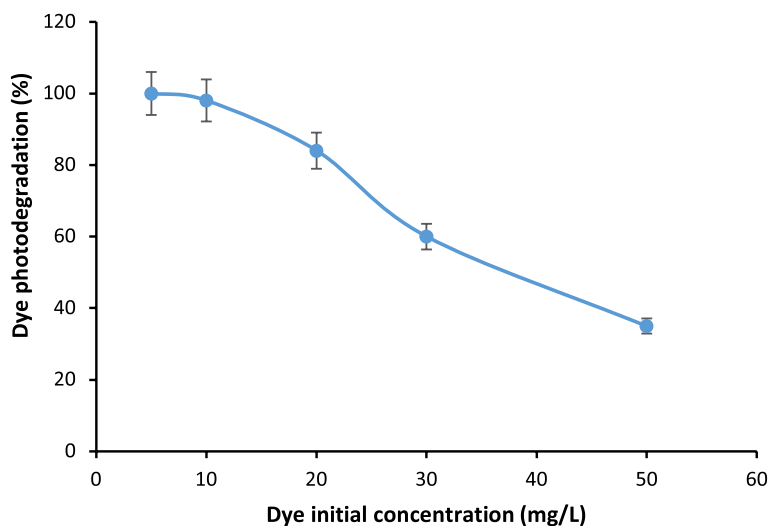

Fig. 11 Effect of the initial dye concentration (dye dye solution volume = 50 mL photocatalyst weight = 40 mg, irradiation time = 60 min, and media pH = 5)
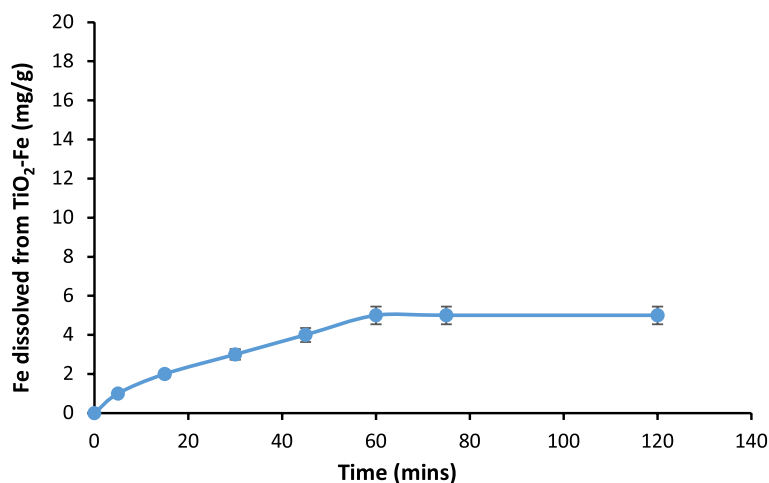
Wahyuni *et al. Journal of Engineering and Applied Science*   (2023) 70:9

Page 13 of 14

Fig. 12 The amount of the Fe dopant dissolved from the doped photocatalyst during the photocatalysis degradation process

Conclusions

It can be concluded that the Fe^{3+} ions dissolved from the iron rusty waste have been successfully doped into TiO_2 structure, which can shift the light absorption into longer wavelengths, and so decreasing the band gap energy (Eg) values, that are categorized in the visible regime. The Eg narrowing is proportional to the amount of Fe dopant, and the most effective Eg reduction is demonstrated by the highest Fe content in the doped-TiO_2 that is TiO_2–Fe (1:1). The Eg decreasing results in the enhanced TiO_2 activity under visible light in the Congo red photodegradation, and the highest activity is found in the TiO_2–Fe (1:0.5). The best condition for the degradation of the 10 mg/L dye concentration in 50 mL solution over TiO_2–Fe (1:0.5) is achieved by using 40 mg of the photocatalyst mass, in 60 min, and at pH 5, that is 99 %. It is clearly inferred that the rusty waste can be utilized for preparing the visible responsive TiO_2 in order to prevent Congo red dye pollution.

Abbreviations
SRUV   Specular reflectance UV/Vis
XRD   X-ray diffraction
FTIR   Fourier transform infrared
TEM   Transmission electron microscopy
Eq.   Equation
Eg   Band gay energy

Availability of data and materials
The data used and/or analyzed during the conduct of this study are available from the corresponding author upon reasonable request.

Declarations

References

1. Amini M, Ashrafi M (2016) Photocatalytic degradation of some organic dyes under solar light irradiation using TiO2 and ZnO nanoparticles. Nano Res 1:79–86. https://doi.org/10.7508/ncr.2016.01.010
2. Zhu X, Zhou D, Cang L, Wang Y (2012) TiO2 photocatalytic degradation of 4-chlorobiphenyl as affected by solvents and surfactants. J Soils Sediments 12:376–385. https://doi.org/10.1007/s11368-011-0464-y
3. Dalida MLP, Amer KMS, Su CC, Lu MC (2014) Photocatalytic degradation of acetaminophen in modified TiO2 under visible irradiation. Environ Sci Pollut Res 21:1208–1216. https://doi.org/10.1007/s11356-013-2003-4
4. Wu S, Hu H, Lin Y et al (2020) Visible light photocatalytic degradation of tetracycline over TiO2. Chem Eng J 382:122842. https://doi.org/10.1016/j.cej.2019.122842
5. Ben Jemaa I, Chaabouni F, Ranguis A (2020) Cr doping effect on the structural, optoelectrical and photocatalytic properties of RF sputtered TiO2 thin films from a powder target. J Alloys Compd 825:153988. https://doi.org/10.1016/j.jallcom.2020.153988
6. Li X, Guo Z, He T (2013) The doping mechanism of Cr into TiO 2 and its influence on the photocatalytic performance. Phys Chem 15:20037–20045. https://doi.org/10.1039/c3cp53531b
7. Kaur R, Singla P, Singh K (2018) Transition metals (Mn, Ni, co) doping in TiO2 nanoparticles and their effect on degradation of diethyl phthalate. Int J Environ Sci Technol 15:2359–2368. https://doi.org/10.1007/s13762-017-1573-y
8. Lee H, Jang HS, Kim NY, Joo JB (2021) Cu-doped TiO2 hollow nanostructures for the enhanced photocatalysis under visible light conditions. J Ind Eng Chem 99:352–363. https://doi.org/10.1016/j.jiec.2021.04.045
9. Crişan M, Drăgan N, Crişan D et al (2016) The effects of Fe, co and Ni dopants on TiO2 structure of sol–gel nanopowders used as photocatalysts for environmental protection: a comparative study. Ceram Int 42:3088–3095. https://doi.org/10.1016/j.ceramint.2015.10.097
10. Khoshnevisan B, Marami MB, Farahmandjou M (2018) Fe3+-doped Anatase TiO2 study prepared by new sol-gel precursors. Chin Phys Lett 35:27501–27505. https://doi.org/10.1088/0256-307X/35/2/027501
11. Matias ML, Pimentel A, Reis-Machado AS et al (2022) Enhanced Fe-TiO2 solar photocatalysts on porous platforms for water purification. Nanomaterials 12:1–23. https://doi.org/10.3390/nano12061005
12. Sood S, Umar A, Kumar S, Kumar S (2015) Journal of colloid and Interface science highly effective Fe-doped TiO 2 nanoparticles photocatalysts for visible- light driven photocatalytic degradation of toxic organic compounds. J Colloid Interface Sci 450:213–223. https://doi.org/10.1016/j.jcis.2015.03.018
13. Zafar Z, Ali I, Park S, Kim JO (2020) Effect of different iron precursors on the synthesis and photocatalytic activity of Fe–TiO2 nanotubes under visible light. Ceram Int 46:3353–3366. https://doi.org/10.1016/j.ceramint.2019.10.045
14. Delekar SD, Yadav HM, Achary SN et al (2012) Structural refinement and photocatalytic activity of Fe-doped anatase TiO 2 nanoparticles. Appl Surf Sci 263:536–545. https://doi.org/10.1016/j.apsusc.2012.09.102
15. Medina-Ramírez I, Liu JL, Hernández-Ramírez A et al (2014) Synthesis, characterization, photocatalytic evaluation, and toxicity studies of TiO2-Fe3+ nanocatalyst. J Mater Sci 49:5309–5323. https://doi.org/10.1007/s10853-014-8234-z
16. Xie W, Ding J, Wei X et al (2019) Corrosion resistance of stainless steel and pure metal in ternary molten nitrate for thermal energy storage. Energy Procedia 158:4897–4902. https://doi.org/10.1016/j.egypro.2019.01.703
17. Babar S, Gavade N, Shinde H et al (2018) Evolution of waste iron rust into magnetically separable g-C3N4-Fe2O3 Photocatalyst: an efficient and economical waste management approach. ACS Appl Nano Mater 1:4682–4694. https://doi.org/10.1021/acsanm.8b00936
18. Jerie S (2016) Occupational risks associated with solid waste management in the informal sector of Gweru, Zimbabwe. J Environ Public Health 1–14. https://doi.org/10.1155/2016/9024160
19. Harja M, Buema G, Bucur D (2022) Recent advances in removal of Congo red dye by adsorption using an industrial waste. Sci Rep 12:1–18. https://doi.org/10.1038/s41598-022-10093-3
20. Sathishkumar K, AlSalhi MS, Sanganyado E et al (2019) Sequential electrochemical oxidation and bio-treatment of the azo dye Congo red and textile effluent. J Photochem Photobiol B Biol 200:111655. https://doi.org/10.1016/j.jphotobiol.2019.111655
21. Tapalad T, Neramittagapong A, Neramittagapong S, Boonmee M (2008) Degradation of Congo red dye by ozonation. Chiang Mai J Sci 35:63–68
22. Dhahir SA, Al-Saade KA, Al-Jobouri IS (2015) Removal of Congo red by photochemical treatment using photo-Fenton reagent. Anal Chem Indian J 15:117–124
23. Shaban M, Abukhadra MR, Ibrahim SS, Shahien MG (2017) Photocatalytic degradation and photo-Fenton oxidation of Congo red dye pollutants in water using natural chromite—response surface optimization. Appl Water Sci 7:4743–4756. https://doi.org/10.1007/s13201-017-0637-y
24. Mironyuk I, Danyliuk N, Tatarchuk T et al (2021) Photocatalytic degradation of Congo red dye using Fe-doped TiO 2 nanocatalysts. Phys Chem Solid State 22:697–710. https://doi.org/10.15330/pcss.22.4.697-710
25. Aprilita NH, Amalia D, Wahyuni ET (2022) Removal of the hazardous Congo red dye through degradation under visible light photocatalyzed by C,N co-doped TiO2 prepared from chicken egg white. Sci World J 2022:14–17. https://doi.org/10.1155/2022/2613841

Publisher's Note